High-Energy Interference Effect of Bremsstrahlung Production in a Single Crystal of Silicon*

A. N. SAXENA†
High-Energy Physics Laboratory, Stanford University, Stanford, California

(Received September 18, 1961; revised manuscript received November 10, 1961)

In an experiment performed at Stanford to look for the interference effect of the bremsstrahlung production by 575-Mev electrons in a single crystal of silicon, the ratio of the charges collected in the two halves of a double ion chamber were used to detect the enhancement of the soft component of the bremsstrahlung. The data, presented in the form of a three-dimensional plot of the ratio vs the angles of rotation between the lattice normal and the electron beam about the horizontal and the vertical axes, clearly showed the enhancement. Comparison of the experimental result and the theory showed good agreement. The resolution of this experiment was poor; hence the central minimum predicted by the theory could not be observed. This minimum, however, has been observed by Bologna *et al.* at Frascati.

I. INTRODUCTION

THE bremsstrahlung spectrum produced by high-energy electrons passing through a thin target of low-Z material is well represented by the Bethe-Heitler[1] formula. However, if the target material is a single crystal, interference effects are to be expected in the production of the bremsstrahlung, This has been discussed by several authors,[2] most recently and in greatest detail by Überall.[3,4] The approximations used by Überall have been critically examined by Schiff.[5] Experiments aimed at checking the predictions of Überall were performed by Panofsky and Saxena[6,7] at Stanford, Frisch, and Olson[8] at Cornell, and Bologna *et al.*[9] at Frascati. The experiments of Bologna *et al.* have verified Überall's predictions for the interference effects in both the pair production and the bremsstrahlung production in the single crystals. The resolutions of these experiments were quite good, which made possible the observation of the central minimum in the bremsstrahlung enhancement peak. The purpose of this paper is to describe the experiment performed at Stanford[7] in detail, and to discuss its comparison with the theory.

* This work was supported by the joint program of the Office of Naval Research, the U. S. Atomic Energy Commission, and the Air Force Office of Scientific Research.

† Now at the Research and Development Department, Fairchild Semiconductor, Palo Alto, California.

[1] H. Bethe and W. Heitler, Proc. Roy. Soc. (London) **A146**, 83 (1934).

[2] E. J. Williams, Kgl. Danske Videnskab. Selskab, Mat.-fys. Medd. **13**, No. 4 (1935); B. Ferretti, Nuovo cimento **7**, 118 (1950); M. L. Ter-Mikaelyan, Zhur. Eksp. i Teoret. Fiz. **25**, 289, 296 (1955); F. J. Dyson and H. Überall, Phys. Rev. **99**, 604 (1955).

[3] H. Überall, Phys. Rev. **103**, 1055 (1956).

[4] H. Überall, CERN Report No. 58-21, September 1958 (unpublished); also, W. K. H. Panofsky (private communication).

[5] L. I. Schiff, Phys. Rev. **117**, 1394 (1960).

[6] W. K. H. Panofsky and A. N. Saxena, Phys. Rev. Letters **2**, 219 (1959).

[7] A. N. Saxena, Phys. Rev. Letters **4**, 311 (1960).

[8] O. R. Frisch and D. N. Olson, Phys. Rev. Letters **3**, 141 (1959).

[9] G. Bologna, G. Diambrini, and G. P. Murtas, Phys. Rev. Letters **4**, 134, 572 (1960).

II. EXPERIMENTAL ARRANGEMENT

In essence, the instrument used to monitor the bremsstrahlung beam and to detect the enhancement was a double ion chamber; the two halves of which were preceded by appropriate thicknesses of Be converters. The relative sensitivity of each half to a given bremsstrahlung spectrum depended on the thickness of the Be converter preceding each ion chamber. A smaller thickness of the Be converter used ahead of the first half of the ion chamber made it sensitive to the softer part of the bremsstrahlung spectrum; the thicker Be converter used ahead of the second half of the ion chamber made it sensitive to the harder component of the bremsstrahlung spectrum. Thus the *ratio* of the charges collected in the two halves of the double ion chamber was a measure of the enhancement of the soft part of the bremsstrahlung.

A. Crystal Target

A single crystal of silicon, cut along the (110) plane, was lapped and etched using standard techniques. It was mounted in a holder which could be rotated to permit its needed alignment by means of an x-ray machine. The Laue back-reflection method was used to align the (110) plane normal to the x-ray beam. The crystal in its holder was next transferred to a goniometer which provided rotational movements about two coplanar orthogonal axes. An optical technique was devised to transfer the x-ray alignment to the electron-beam alignment of the Mark III linear accelerator. Thus the lattice normal was made parallel to the incident electron beam at the central angle setting.

B. Double Ion Chamber

Figure 1 shows the basic construction of this instrument. As the name implies, it consisted of two ionization chambers enclosed in one envelope. The two ion chambers were identical in construction, hence only one of them will be described. Various parts of the second ion chamber have been identified by primed letters

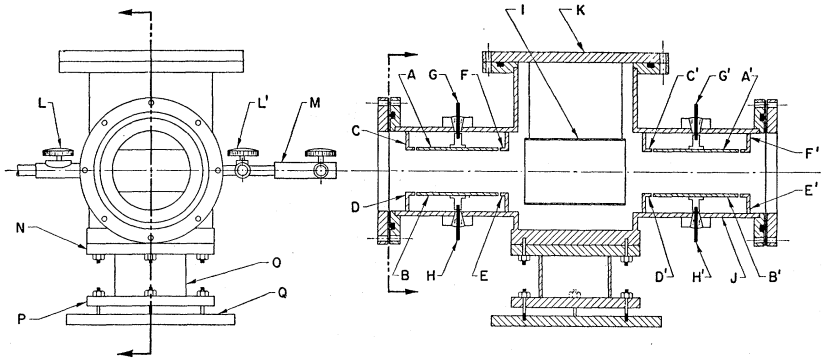

FIG. 1. The double ion chamber.

corresponding to their counterparts of the first ion chamber.

The first ion chamber consisted of two parallel plates A and B, suspended from two Kovar seals G and H which were welded to the envelope J. The size of each plate was 3 in.×4 in., and the distance between them was 2 in. Angles C, D, E, and F were welded to the envelope J to serve as guard rings for the plates A and B in the axial direction of the instrument. From the top lid K hung a holder I in which varying thicknesses of Be disks would be interposed between the two ion chambers. The lid sealed the instrument when clamped against an O-ring in the upper flange. At the ends two dural windows were provided. Valves L, L′ and M were also provided to allow H_2 to flow through the double ion chamber. The H_2, which was purified by passing it through a de-oxo unit and liquid N_2 trap, flowed through the chamber at constant pressure.

The double ion chamber was mounted on a stand O which allowed rotational (at N), vertical (at P), and transverse (at Q) adjustments to be made in its alignment.

C. Electronics

The low level of the currents ($\sim$0.1 μa) from the ion chambers were amplified by a suitably designed dc amplifier with an electrometer tube as the input stage. Two such amplifiers were constructed in one chassis. The outputs of the two amplifiers were connected across two helipots, and the ratio of the currents was observed by the balanced potentiometer method. The ratio of the resistances involved gave the ratio of the desired currents.

D. Experimental Method and Arrangement

The layout of the experiment is shown in Fig. 2. The electron-beam exit in the end-station of the linear accelerator was sealed off by a 2-mil dural window at the mouth of the bunker wall. Next down the line was the crystal mounted in the goniometer. Both directions of rotation of the crystal about the horizontal and vertical axes were motorized and remote-controlled. The (110) plane of the silicon crystal was normalized by means of x-ray and optical techniques.

A ditching magnet was placed after the goniometer to deflect the electrons away from the photon beam into a secondary electron-emission monitor. The last instrument down the line was the double ion chamber, mounted on its stand.

E. Data and the Experimental Results

Electrons of 575 Mev produced bremsstrahlung in the single crystal of silicon with its (110) plane initially normal to the electron beam. The thickness of the Be converter penetrated by the bremsstrahlung ahead of the first ion chamber was 2 in. (0.147 radiation length) and that ahead of the second ion chamber was 6.5 in. (0.478 radiation length). The ratio of the charges collected in the two ion chambers, which is a measure of the enhancement, was observed for various angles as the crystal was rocked back and forth about the vertical and horizontal axes. An angular grid of about $\pm$16 min of θ_v, the rotation about the vertical axis, and about $\pm$48 min of θ_h, the rotation about the horizontal axis, was covered in steps of 4 min. The data, taken from an earlier report,[7] are shown in Fig. 3 in a three-dimensional plot of the ratio vs θ_v and θ_h. The peak shows clearly the enhancement of the soft part of the bremsstrahlung.

III. THEORETICAL ESTIMATION OF THE RATIO

Some of the γ rays get converted in the Be disks placed ahead of the ion chambers and produce electrons and positrons, and the charges due to these are observed in the ion chambers. The efficiency of the chambers is calculated as follows:

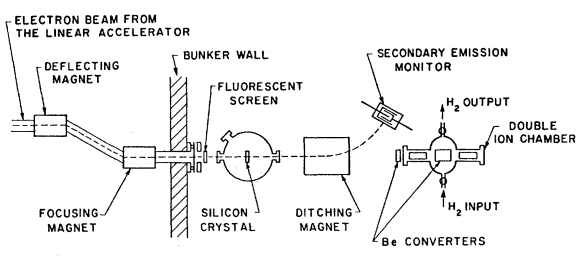

FIG. 2. The layout of the experiment.

(1) Calculate the number of electrons and positrons produced by pair production by a γ ray of energy k Mev at a given depth of Be and of sufficient energy to emerge from that depth. In this calculation, we take into account the straggling in the energy losses of the charged particles by radiation and average ionization loss.

(2) Calculate the number of knocked-on electrons by the Compton scattering of a γ ray of energy k Mev. In this calculation, we take into account only the average total energy loss of the electron.

Neglect the secondary processes because their contribution is small.

A. Straggled Pairs

Consider a Be converter of thickness t. Let N_{k_0} = number of incident photons of energy k_0, σ_P = pair production cross section at photon energy k_0, σ_C = Compton scattering cross section at photon energy k_0, $\sigma=\sigma_P+\sigma_C$. Then, $\sigma_P N_{k_0} e^{-\sigma x} dx$ = number of pairs produced at a depth x (measured in atoms/cm^2) in the Be converter.

Assume that the energy spectrum of the pair fragments produced is flat. Let the energy of an electron be E, and let the average ionization energy loss be a. The minimum energy of the electron at depth x should be $a(t-x)$ in order that it will come out of the total thickness t. These electrons will also lose their energy by radiation and thereby have straggling in their energy losses. Using Heitler's[10] radiation straggling function W, the total number of electrons and positrons emerging out of the Be converter of thickness t per incident photon of energy k_0, is

$$\eta^t_{\text{pair}}=[(N_+ + N_-)/N_{k_0}]^t_{\text{pair}} = \frac{2a\sigma_P}{k_0}\int_L^t e^{-\sigma x} 1.193p \times\left[I(p-1, y_0)e^{y_0}-\frac{{y_0}^p}{\Gamma(p+1)}\right]dx, \quad (1)$$

where

$$p=(t-x)/1.193, \quad (2)$$

$$I(p-1, y_0)=\gamma(p,y_0)/\Gamma(p), \quad (3)$$

$$y_0=\ln(k_0/1.193ap), \quad (4)$$

$\gamma(p,y_0)$ is the incomplete gamma function defined as

$$\gamma(p,y_0)=\int_0^{y_0} e^{-Z} Z^{p-1} dZ. \quad (5)$$

[10] W. Heitler, *The Quantum Theory of Radiation* (Clarendon Press, Oxford, England, 1954), 3rd ed., p. 379.

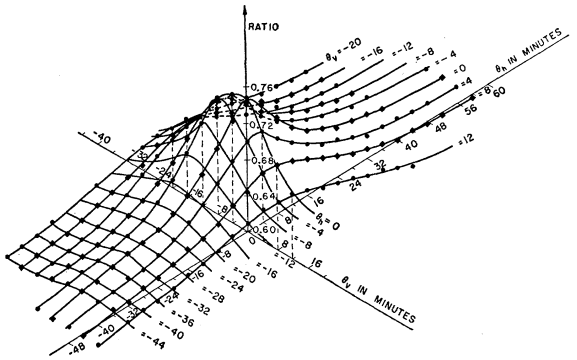

FIG. 3. Plot of the ratio of the charges collected in the two ion chambers, which is a measure of the enhancement vs θ_v, the rotation about the vertical axis, and θ_h, the rotation about the horizontal axis.

The functions $I(p-1, y_0)$ are tabulated in Pearson's tables[11] and those compiled by Walton *et al.*[12]

In Eq. (1), the lower limit L is defined as

$$\begin{aligned} L&=0 \quad \text{if} \quad t<k/a, \\ L&=t-(k/a) \quad \text{if} \quad t>k/a. \end{aligned} \quad (6)$$

The integral in Eq. (1) was computed numerically for the two thicknesses of Be and for various photon energies. Figure 4 shows a plot of η^t_{pair} vs k_0 for the two thicknesses of the Be converter.

B. Compton Knocked-on Electrons

The differential cross section $d\sigma_C$ for the Compton scattering of a photon of primary energy k_0 into the energy range from k to $k+dk$, neglecting the higher order terms, is given by[13]

$$d\sigma_C \cong \pi r_0^2 \frac{mc^2}{k_0}\frac{dk}{k}\left[1+\left(\frac{k}{k_0}\right)^2\right]\frac{N_0 Z}{A} \text{ cm}^2/\text{g}, \quad (7)$$

where r_0 = classical radius of the electron, m = electron mass, c = velocity of light, N_0 = Avogadro's number, Z = atomic number (of Be, in this case), and A = atomic weight (of Be, in this case).

Neglecting the radiation straggling, the total number of electrons emerging out of the Be converter of thickness t per incident of photon energy k_0 is

$$\eta^t_{\text{Compton}}=(N^-/N_{k_0})^t_{\text{Compton}} = C_{k_0}\int_L^t e^{-\sigma x}\left\{\ln\left[\frac{k_0-E(\xi)}{k_{\min}}\right] + \frac{[k_0-E(\xi)]^2-{k_{\min}}^2}{2{k_0}^2}\right\}dx, \quad (8)$$

[11] K. Pearson, *Tables of the Incomplete Gamma Function* (Cambridge University Press, New York, 1951).

[12] J. R. Walton, T. Sikkeland, A. Ghiorso, and G. T. Seaborg, University of California, Lawrence Radiation Laboratory, Report No. UCRL-9107, 1960 (unpublished).

[13] H. Bethe and J. Ashkin, *Experimental Nuclear Physics*,

where

$$C_{k_0}=\pi r_0^2(mc^2/k_0)(N_0Z/A), \tag{9}$$

$$k_{\min}=k_0/[1+(2k_0/mc^2)], \tag{10}$$

and

$$\xi=t-x$$

$$=-\int_0^{E(\xi)}\frac{dE}{(1/\rho)(dE/dx)_{\text{total}}}\ \text{g/cm}^2; \tag{11}$$

i.e., ξ is the "range" of an electron of energy $E(\xi)$.

The value of $k_0>E(\xi)$ determines L, the lower limit of the integral over x. For a given t, if $k_0>E(\xi)$, then $L=0$. If $k_0<E(\xi)$, then $L=$the x value corresponding to $E(\xi)=k_0$. At this singularity, the value of the integral was taken to be zero. The integral in Eq. (8) was computed numerically. Figure 4 shows a plot of η^t_{Compton} vs k_0 for the two thicknesses of the Be converter.

In the above calculation, the higher order terms of the Klein-Nishina formula

$$C_{k_0}\left[-\frac{2(\gamma+1)}{\gamma^2}+\frac{1+2\gamma}{\gamma^2}\frac{k}{k_0}+\frac{1}{\gamma^2}\frac{k_0}{k}\right]\frac{dk}{k}, \tag{12}$$

were nelgected, since the calculation shows that the effect of these terms on η^t_{Compton} was negligible.

It was also found that the contribution of the electrons from the photoelectric effect $\eta^t_{\text{photoelectric}}$ was negligible.

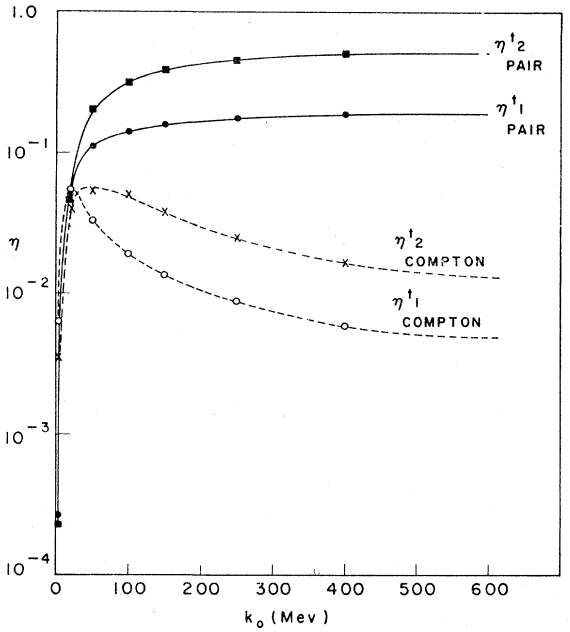

FIG. 4. Plot of η^t_{pair} and η^t_{Compton} vs k_0 for the two thicknesses t_1 (0.147 radiation length) and t_2 (0.478 radiation length) of the Be converters used.

edited by E. Segrè (John Wiley & Sons, Inc., New York, 1953), Vol. 1, p. 320.

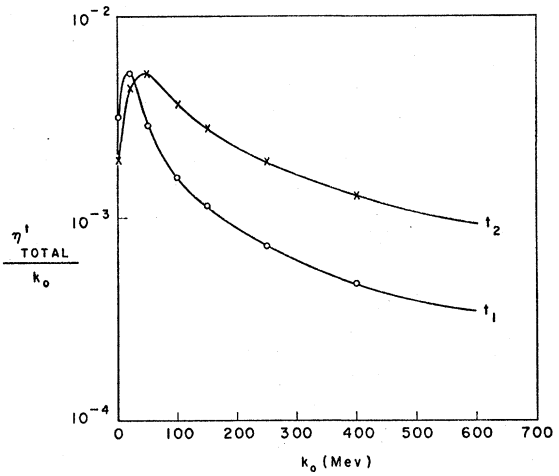

FIG. 5. Plot of $\eta^t_{\text{total}}/k_0$ vs k_0 for the two thicknesses t_1 (0.147 radiation length) and t_2 (0.478 radiation length) of the Be converters used.

Figure 5 shows the plot of $\eta^t_{\text{total}}/k_0$ vs photon energy k_0 for the two thicknesses of the Be converters used, where

$$\eta^t_{\text{total}}=\eta^t_{\text{pair}}+\eta^t_{\text{Compton}}. \tag{13}$$

It should be noticed that the peak in Fig. 5 for t_1 occurs at a softer photon energy than that for t_2. As discussed above, in the thin Be converter (t_1), hard radiation will produce, relatively speaking, a smaller number of electrons than in t_2, and therefore it will be relatively more sensitive to the soft radiation.

C. Theoretical Ratio

In the experiment performed, the charge collected in each ion chamber is approximately proportional to the ionization produced by the entire bremsstrahlung spectrum in the Be converters. Therefore, the charge collected by the ion chamber $A_t{}^{\text{U}}(\theta)$ is given by

$$A_t{}^{\text{U}}(\theta)\propto\int_{k_{\min}}^{k}\frac{\eta^t_{\text{total}}}{k}\frac{k\sigma^{\text{U}}(\theta)}{E_1\bar{\sigma}}dk, \tag{14}$$

where the superscript U refers to the Überall spectrum, and $\eta^t_{\text{total}}=$the total number of electrons and positrons produced in a Be converter of thickness t by a photon of energy k Mev, $\sigma^{\text{U}}=$the Überall cross section for the interference bremsstrahlung spectrum produced by high-energy electrons in a single crystal, $\bar{\sigma}=Z^2r_0^2/137$, $E_1=mc^2$, and $\theta=$the angle between the lattice vector and the electron beam. We obtained $k\sigma^{\text{U}}/E_1\bar{\sigma}$ for silicon by scaling the corresponding quantity, calculated and plotted by Überall, for copper.[3] This is discussed in the appendix. Equation 14 was integrated numerically for the two thicknesses of Be and for various angles θ.

IV. CORRECTIONS

A. Additional Radiator in the Beam

We must correct for the additional radiation length involved, other than that of the silicon crystal, such as aluminum windows and air in the path of the electron beam. The theoretical ratio also must be modified because of the multiple scattering of the electrons, the latter to be discussed in the next section. The bremsstrahlung spectrum produced in the additional radiation length described above follows the Bethe-Heitler formula.[1] Therefore, the charge in the ion chamber due to this additional thickness is given by

$$A_t^{\text{B-H}} \propto \int_{k_{\min}}^{k_0} \frac{\eta^t{}_{\text{total}}}{k} \frac{k\sigma^{\text{B-H}}}{E_1\bar{\sigma}} dk, \tag{15}$$

where the superscript B-H refers to the Bethe-Heitler spectrum, and $\sigma^{\text{B-H}}$ is the Bethe-Heitler cross section for the bremsstrahlung spectrum produced by high-energy electrons. (Since $\sigma^{\text{B-H}}$ is independent of θ, $A_t^{\text{B-H}}$ also does not have any angular dependence.)

Let N = the number of atoms/cm^3, and x = the thickness of the radiator in cm. Then the theoretical ratio of the charges in the ion chambers for the (110) plane of the silicon crystal would be given by

$$R(\theta)=\frac{(N_{\text{Al}}x_{\text{Al}}+N_{\text{air}}x_{\text{air}})A_{t_1}^{\text{B-H}}+1.41N_{\text{Si}}x_{\text{Si}}A_{t_1}^{\text{U}}(\theta)}{(N_{\text{Al}}x_{\text{Al}}+N_{\text{air}}x_{\text{air}})A_{t_2}^{\text{B-H}}+1.41N_{\text{Si}}x_{\text{Si}}A_{t_2}^{\text{U}}(\theta)}. \tag{16}$$

Figure 6 shows a plot of $R(\theta)$ vs θ.

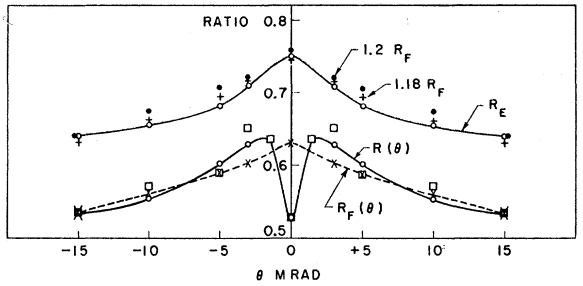

FIG. 6. Plot of the following quantities vs θ. The curve marked $R(\theta)$ is that given by Eq. (16), and is the theoretical unfolded curve for the ratio derived from Überall's theory. The square points (⊡) are those of a function, $f(\theta)=0.527+0.072\theta^2 \times\exp(-0.2\theta^2)+0.003\theta^2\exp(-0.02\theta^2)$, used to fit the $R(\theta)$ curve. The dashed curve drawn through the points marked by crosses (×) is $R_F(\theta)$, the folded curve in which the total multiple scattering angle used is 1.95 mrad. $R_E(\theta)$ is the experimental ratio curve obtained from the data in Fig. 3 for various values of θ_v at $\theta_h=0$. The solid circles are the points obtained from the experimentally normalized R_F curve, $1.2R_F$, when the normalization was done with an experimental ratio point taken at $\theta=40$ mrad. Points shown by pluses (+) indicate the theoretically normalized R_F curve, $1.18R_F$, when the multiple scattering in the Be converter is also taken into account.

B. Multiple Scattering of the Incident Beam

The incident electrons undergo multiple scattering as they pass through the single crystal target and also the additional radiation length present in the experimental setup. Thus the multiple scattering of the electrons has to be folded into Eq. (16).

The multiple scattering of electrons in passing through a single crystal involves small momentum transfers; therefore, one could expect coherence effects here as well. Whenever such a momentum transfer corresponds to the reciprocal lattice vector of the crystal plane, interference would occur at an angle defined by the momentum transfer. Thus, Molière's theory[14] may not hold for the crystalline targets. This motivated us to measure the multiple scattering angle experimentally.

In the following treatment, the symbol Y is used to denote the variance expressed in units of length of the density distribution function of the beam spot, and the symbol σ is used to denote the same expressed in units of angle.

Procedure

Beam-spot pictures were taken by exposing plain glass slides at three positions A, B, and C with and without the crystal in between the positions A and B. Figure 7 illustrates the geometry of the experimental setup. These beam-spot pictures were scanned by a densitometer and Y_{obs} determined from the density distribution curves.

When the crystal is "out," the contribution to Y_{obs} is from the following sources:

(1) Multiple scattering of the electrons in the radiation length present before the plate where the beam-spot picture was taken. Let us denote this by Y_{scatt}.

(2) Focussing and deflecting magnets' optics. (a) Finite size of the beam; (b) $\Delta E/E$ of the beam. Let us denote the contribution from both (a) and (b) by Y_{div} and call it the contribution from the beam divergence. Thus we have the following relations:

$$^AY_{\text{obs}}{}^2={}^AY_{\text{scatt}}{}^2+{}^AY_{\text{div}}{}^2, \tag{17}$$

$$^BY_{\text{obs}}{}^2={}^BY_{\text{scatt}}{}^2+{}^BY_{\text{div}}{}^2, \tag{18}$$

$$^CY_{\text{obs}}{}^2={}^CY_{\text{scatt}}{}^2+{}^CY_{\text{div}}{}^2 \tag{19}$$

Using these equations and the geometrical relationship between $^AY_{\text{div}}$, $^BY_{\text{div}}$ and $^CY_{\text{div}}$, the beam divergence in angles, denoted by σ_{div}, was found to be 1.58 mrad. This agrees with the angular divergence of the beam emerging from the focussing system, calculated by using the formula given by Brown[15] and the pole-tip settings of the magnets.

When the crystal is "in," the beam-spot pictures at the positions B and C might have an additional contri-

[14] G. Molière, Z. Naturforsch. **2A**, 133 (1947); **3A**, 78 (1948).
[15] K. L. Brown, Rev. Sci. Instr. **27**, 959 (1956).

bution to the Y_{obs} which could probably come from the coherent multiple scattering of the crystal. Let this additional term be denoted by Y_ϵ. Therefore, we have

$$^BY_{obs}{}^{2\prime}=\,^BY_{scatt}{}^{2\prime}+\,^BY_{div}{}^{2\prime}+\,^BY_\epsilon{}^2, \quad (20)$$

$$^CY_{obs}{}^{2\prime}=\,^CY_{scatt}{}^{2\prime}+\,^CY_{div}{}^{2\prime}+\,^CY_\epsilon{}^2. \quad (21)$$

The primes denote the crystal-in case.

The contribution from the coherent multiple scattering expressed in angles σ_ϵ, as postulated above, was evaluated from Eqs. (20) and (21). Figure 8 shows the plot of $^B\sigma_\epsilon$ vs θ_v, the angle between the electron beam and the lattice vector. It is clear from this figure that there is no systematic variation of σ_ϵ as θ_v is changed. This is more obvious because the curve is asymmetric about the $\theta_v=0$ ordinate. However, the average value of σ_ϵ is not zero which then indicates that there could be some contribution from the coherent multiple scattering of the electron beam in the single crystal. This result should be considered as tentative since no check in which a noncrystalline target of equivalent radiation length was substituted for the silicon crystal could be carried out.

The errors shown in the curve of Fig. 8 are those in the measurements of Y_{obs} and an assumed error of 20% in the calculated values of $Y_{scatt}{}^2$, both propagated properly through the algebra of evaluating Y_ϵ and σ_ϵ.

The total projected multiple scattering angle to be used in the folding calculation was evaluated from

$$\sigma_{total}{}^2=\sigma_{scatt}{}^2+\sigma_{div}{}^2+\sigma_\epsilon{}^2 \quad (22)$$

and σ_{total} was found to be 1.95 mrad.

V. COMPARISON OF THE THEORETICAL AND OBSERVED RATIOS

The curve $R(\theta)$ vs θ, given by Eq. (16) and shown in Fig. 6, was fitted by a function of the form $c+a\theta^2\times\exp(-b\theta^2)$ and a folding calculation was made using the total multiple scattering angle σ_{total} given by Eq. (22). Figure 6 also shows the folded curve $R_F(\theta)$

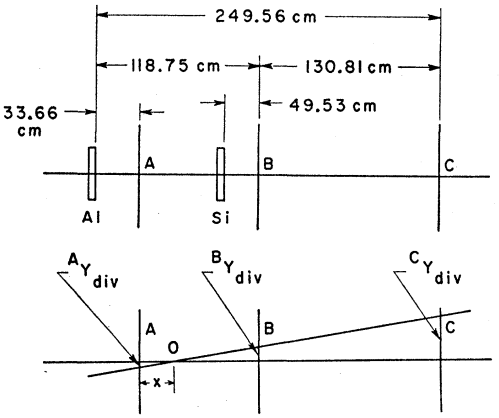

FIG. 7. Schematic diagrams of the beam-spot pictures taken for the estimation of the multiple scattering.

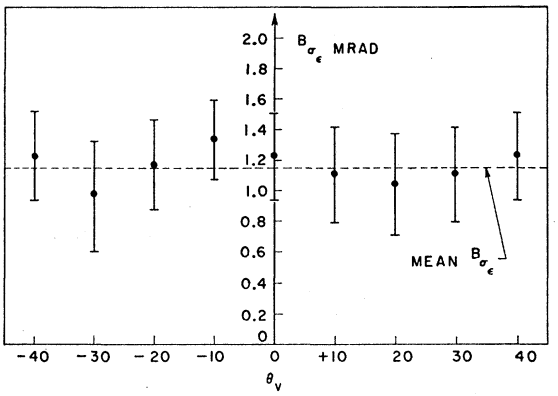

FIG. 8. Plot of $^B\sigma_\epsilon$, the postulated coherent multiple scattering angle in the single crystal of silicon, vs θ_v at $\theta_h=0$.

which can be compared with the experimental curve $R_E(\theta)$. It is observed that the net enhancement is the same in the two curves R_E and R_F except that the curve R_E is shifted above R_F. However, if the data of the curve R_E are normalized at a point taken at $\theta=40$ mrad, where the Überall spectrum is similar to the Bethe-Heitler spectrum, R_F shifts up closer to R_E. The normalization gives for the theoretical value of the ratio $1.2R_F$. Figure 6 also shows the normalized ratio R_N which is $1.2R_F$. Good agreement is observed between R_N and R_E.

Making use of the fact that the electrons also undergo multiple scattering in the Be converters and thus some of the electrons produced in the first converter miss the second ion chamber, we made an approximate calculation to determine the normalization constant. This gave the value of the constant as 1.18. Thus the agreement between theory and experiment is good.

ACKNOWLEDGMENTS

The author is deeply indebted to Professor W. K. H. Panofsky for his advice and encouragement throughout the progress of this work. The help of Professor L. I. Schiff and Professor H. C. DeStaebler, Jr., and several colleagues in this laboratory is gratefully acknowledged.

APPENDIX

Considering the basic limits on the accuracy of this experiment, it was not considered worthwhile to compute the theoretical cross section according to Überall specifically for silicon. Rather an interpolation method was adopted starting from the Überall's published computations for copper.

To reduce 1 Bev copper data to 575 Mev curve, the angles θ corresponding to a fixed $k\sigma/E_1\bar{\sigma}$ were multiplied, as a first approximation, by the ratio of the energies 1000/575. This was done because the higher the primary electron energy, the smaller the θ will be at which the maximum of the bremsstrahlung peak would occur. [As an example, in Fig. 11(b) of Überall[3]

for 1 Bev, the peak for $x=0.2$ occurs at about 2 mrad. For the same $x=0.2$ in Fig. 10(b) for 200 Mev incident electrons, the peak occurs at about 10 mrad which agrees with the value obtained by above procedure, viz, $2\times(1000/200)=10$ mrad]. Further, changing the atomic number Z in going from copper to silicon, and the lattice spacing a has two effects: (1) The cross section scales with the quantity $\alpha Z^2 r_0^2$. The scaling constant will cancel out when the ratio of the charges is taken [see Eqs. (14)–(16)]. (2) The same coherence effects would be expected for a given value of qa, where q is the momentum transfer. Hence, to first order, the scale of angles should be multiplied by the ratio of the lattice constants. It is this procedure[16] which was used in converting the Überall curves from 1-Bev copper data to the 575-Mev silicon curve.

A more precise method[17] is based on interpolating the various functions (ψ_1^c; ψ_1^0; ψ_2^c; ψ_2^0) as used in the original paper.[3] The procedure is as follows:

Write the cross section as

$$\sigma=\bar{\sigma}(dx/x)\{[1+(1-x)^2][\psi_1^c(\delta)+\psi_1^0(\delta,\theta)] -\tfrac{2}{3}(1-x)[\psi_2^c(\delta)+\psi_2^0(\delta,\theta)]\}, \quad \text{(A1)}$$

where $x=k/\epsilon_1$, $k=$photon energy, $\epsilon_1=$incident electron energy in units of $mc^2=1125$ for the present case, and $\delta=(1/2\epsilon_1)[x/(1-x)]$.

1. The continuous spectrum is given by the functions ψ_1^c and ψ_2^c, which are approximated as, using mean-value theorem,

$$\psi_1^c\cong 4\exp(-A\bar{q}^2)+4[1-\exp(-A\bar{q}^2)]\times[\Phi_1-\tfrac{4}{3}\ln Z], \quad \text{(A2)}$$

$$\psi_2^c\cong(10/3)\exp(-A\bar{q}^2)+4[1-\exp(-A\bar{q}^2)]\times[\Phi_2-\tfrac{4}{3}\ln Z], \quad \text{(A3)}$$

where the various terms are defined in the original paper by Überall.[3] The value of A for Si at $T=273°$ is 261. The nearest value of A in Überall's calculation is for Cu at 77°, which is $A_{\mathrm{Cu}}=167$. To find a good value of $\bar{q}$, the following procedure was adopted. From Fig. 6 of Überall's paper,[3] the value of ψ_1^c, ψ_2^c, $\Phi_1-\frac{4}{3}\ln Z$ and $\Phi_2-\frac{4}{3}\ln Z$ were read off for $\mu=0$ and $\mu=2$. These values were substituted in Eqs. (A2) and (A3) with the A_{Cu} and the mean value of $\bar{q}^2$ was evaluated; and it was found to be 11.68×10^{-4}. Using this $\bar{q}$ and the A and Z for Si, ψ_1^c and ψ_2^c for Si were obtained and plotted as a function of δ.

2. To evaluate the interference part given by $\psi_1^0(\delta,\theta)$ and $\psi_2^0(\delta,\theta)$, the following two procedures were tried. From Figs. 2–4 of Überall,[3] $\mu\psi_1^0$ and $\mu\psi_2^0$ were read off a given τ for the following five cases: Cu at 0°, 77°; diamond; Pt at 0°, 77°. Corresponding values for these of A are 121.1, 167, 108.4, 55.2, 92.2, respectively. $\mu\psi_1^0$ and $\mu\psi_2^0$ were plotted vs A with the intention of extrapolating them to $A=261$ for Si. The extrapolation was difficult as $\mu\psi_1^0$ and $\mu\psi_2^0$ varied irregularly with A.

The second procedure to obtain the curves of $\mu\psi_{1,2}^0(\tau)$ for Si was quite simple. The $\mu\psi_{1,2}^0(\tau)$ curves for Cu at 77°, were multiplied by $[1-\exp(-261\bar{q}^2)]/[1-\exp(-167\bar{q}^2)]$ to give $\mu\psi_{1,2}^0(\tau)$ for Si.

Finally, from the curves $\psi_{1,2}^c$ vs δ and $\mu\psi_{1,2}^0$ vs τ, $x\sigma/\bar{\sigma}$ was calculated for various x using Eq. (A1).

The agreement between the curves obtained by using the approximate procedure and Überall's procedure was good for large θ. For small θ, e.g., at $\theta=5$ mrad, the curves resulting from the first approximation were shifted above the Überall curves by about 15%. This shift is in the right direction because in the energy scaling of the curve, the ordinates were left alone in the first approximation and only the angles were multiplied by the ratio of the incident electron energies. The ordinates $k\sigma/E_1\bar{\sigma}$ will shift slightly to a smaller value for smaller E_1 at fixed k/E_1. Since this correction is complicated, though small, it was not done and hence the curves resulting from the first approximation were shifted slightly above the Überall curves. However, this did not change the ratio $R(\theta)$, the quantity under consideration in the present experiment. For $\theta=5$ mrad, the ratio $R(\theta)$ using Überall's curve was 0.597, whereas its value using the approximate procedure was 0.601. Since the ratio $R(\theta)$ is insensitive, the approximate procedure was used.

[16] W. K. H. Panofsky (private communication).
[17] H. Überall (private communication).